



# Metal-free nitrogen-rich carbon foam derived from amino acids for the oxygen reduction reaction

Anna Ilnicka<sup>1,\*</sup> , Piotr Kamedulski<sup>1</sup> , Malgorzata Skorupska<sup>1</sup> , and Jerzy P. Lukaszewicz<sup>1,2</sup> 

<sup>1</sup> Faculty of Chemistry, Nicolaus Copernicus University, Gagarina 7, 87-100 Toruń, Poland

<sup>2</sup> Centre for Modern Interdisciplinary Technologies, Nicolaus Copernicus University, Wilenska 4, 87-100 Toruń, Poland

Received: 1 June 2019

Accepted: 22 August 2019

Published online:

6 September 2019

© The Author(s) 2019

## ABSTRACT

The following paper presents the synthesis of nitrogen-rich carbon foams (N-CFO) from amino acids through their thermal decomposition in the presence of solid and removable nanoparticles (template). N-CFO were synthesized by carbonizing L-lysine as the carbon phase precursor and using a hard template of CaCO<sub>3</sub> (added as nano-sized powder). The carbonization process was carried out in a temperature range of 700–900 °C, under the flow of nitrogen. The results show that the textural and chemical properties among other nitrogen content of the N-CFO can be controlled by manipulating carbonization temperature. The obtained N-CFO were either micro- or mesoporous matrixes (open porosity) with high nitrogen content in the range from 4.1 to 12.4 wt%. The walls of the produced N-CFO had a thickness up to 10 nm. The metal-free catalysts such as N-rich carbon foams are valuable materials in oxygen reduction reaction, which is a key reaction for metal–air batteries. It was found that a four-electron reduction process is predominant.

## Introduction

In recent years, the systematic study of nitrogen-rich carbon foam synthesis has drawn a lot of interest to the science and technology of carbon materials. Until now, the focus of nitrogen-containing carbon foam preparation research was placed on the use of synthetic polymers containing nitrogen and their treatment by carbonization in oxygen-free conditions [14, 36]. Currently, the leading direction in nitrogen-rich activated carbon synthesis is the utilization of bio-resources and carbonization of organic

precursors containing nitrogen. An example of this is the use of chitin [12], chitosan [11, 21, 32], *Chlorella vulgaris* [13], and gelatin [8, 23]. N-rich, high-surface-area carbon foams can be prepared using different methods, but most of them are time-consuming and expensive. Therefore, these carbons necessitate a reasonable balance between nitrogen content and the cost of production.

Carbon foam (CFO) is a unique structure among all other known carbon material morphologies, such as fibrous, tubular, spherical, and planar forms. A CFO has a specific pore structure, which overall consists of

Address correspondence to E-mail: ailnicka@umk.pl

open and often interconnected pores, separated by walls in which carbon is the main constituent. Thanks to this kind of structure, CFO has a large surface area and is lightweight and often thermally stable [52]. Unlike ordinary foam structure materials, the low thermal conductivity, along with a high resistance to fire, makes carbon foam a promising candidate for commercial thermal insulation materials [47]. In real CFO, the wall thickness should be comparable to or lower than the size of dominating pores. This ratio differentiates CFO from other carbon-based porous materials, in which pore size is much smaller than the fleshiness of the carbon matrix. The preparation processes of carbon foams comprise a few typical approaches: blowing of carbon precursors followed by carbonization, template carbonization of carbon precursors, compression of an exfoliated graphite assembly of graphene nanosheets, and others [16]. In recent years, the preparation of CFO has been widely reviewed [15, 16, 31, 33]. Certain synthesis approaches actually combine several factors that provide foaming action. Ultra-thin-walled, nitrogen-rich carbon foams (N-CFO) can be fabricated through the pyrolysis of polyimide where graphene is additionally used as a component to stabilize the porous structure and accelerate polyimide graphitization [25]. In a different paper, CFO of high mechanical strength was obtained from coal pitch modified with cinnamaldehyde and boric acid via pretreatment foaming and carbonization [27]. Acid-induced polymerizations of bis(*p*-methoxybenzyl) carbonate, bis(*m*-methoxybenzyl) carbonate, and difurfuryl carbonate made it possible to produce resin foams, thanks to the controlled release of carbon dioxide during the polymerization of these organic carbonates [41].

Carbon foams have been studied regarding certain emerging applications: thermal energy storage, electrode manufacturing for electrochemical energy devices [44, 50], separation of gaseous species (molecular sieving effect), cleanup and recovery of spilled oils, and the reflection of electromagnetic waves. In the case of an electrochemical application (CFO as electrode material), CFO electric conductivity is crucial and usually controlled by heat treatment performed at elevated temperatures. Solving the major problem of preparing CFO would allow successful testing of the electrochemical applicability of graphene-based foams (electrode material) in supercapacitors [5, 39], solar cells [45], and lithium-ion

batteries [24]. Some reports documented the advantages of N-enriched CFO over other electrode materials, e.g., Pt-doped carbon-based electrode materials [46]. The cathodic oxygen reduction reaction (ORR) is a key process in fuel cells [2] and metal–air batteries [40]. Pt-based electrocatalysts have been commonly used in commercial fuel cells, owing to their properties such as high current density and relatively low overpotential [35]. In general, noble-metal-based catalysts have a high intrinsic catalytic activity in sluggish electrochemical reactions, e.g., oxygen reduction reactions (ORR), oxygen evolution reactions (OER), and hydrogen evolution reactions (HER); unfortunately, they are expensive and often susceptible to crossover effects [26]. A possible commercially viable solution lies in substituting noble-metal catalysts with metal-free catalysts. Carbon-based catalysts in particular have stimulated enormous interest due to their abundance, low cost, and environmental friendliness. Furthermore, both theoretical and experimental studies have shown that functionalizing of nano-structured carbon-based materials with heteroatom dopants, such as nitrogen, phosphorus, sulfur, and boron, metal/metal oxide clusters, would improve both electrochemical properties and catalytic activities [10, 17–19, 26, 28–30, 38, 42, 43, 48, 49, 51]. An analysis of the literature revealed that there is still space for new synthesis approaches focused on the preparation of a new class of tiny-walled N-CFO using unconventional raw materials. The present work aims to elaborate on synthesis pathways for obtaining molecularly tiny-walled N-CFO using renewal resources.

The work proposes the application of a bio-originated precursor, i.e., amino acid (*L*-lysine), as a precursor for preparing nitrogen-rich carbon foams. In this process, carbon foams with a very high nitrogen concentration can provide a highly promising metal-free electrocatalyst for ORR in an alkaline medium. The application of amino acids as a precursor for N-CFO manufacturing has not been widely reported yet. The applied amino acids are easily accessible and industrially produced in a large scale. Thus, the current synthesis approach is potentially expandable and cost efficient. These nitrogen-rich carbon foams, with mesopores and a large surface area, were synthesized through a one-step synthesis strategy using calcium carbonate as a template. In an ORR experiment performed in an alkaline medium, the N-CFO

showed comparable electrocatalytic activity to the commercial Pt/C catalyst. These results suggest the possibility of application of N-CFO as an electrocatalyst for Zn–air or Li–air batteries.

## Experimental section

### Material preparation

In the synthesis procedure, 40 g of L-lysine powder (Myprotein) was added to 20 g of particle  $\text{CaCO}_3$  (SkySpring Nanomaterials, size of particle 15–40 nm) and stirred mechanically. 100 cm<sup>3</sup> of distilled water was added to the resulting mixture, which was then placed into a magnetic stirrer for 1 h. To evaporate the distilled water, the mass was dried in an electric furnace at 80 °C for 24 h. In the next step, the mixture of L-lysine and  $\text{CaCO}_3$  was heated up under the flow of nitrogen at a rate of 10 °C min<sup>-1</sup>, until it reached the carbonization temperature range of 700–900 °C; it was held for 1 h at this temperature in a tube furnace (Thermolyne F21100). The prepared samples were cooled to approximately 60 °C (remaining under continuous nitrogen flow). After carbonization, they were treated with a concentrated (34–37%) HCl solution for 20 min (12 ml of acid was used per 1 g of carbon) and then washed with distilled water on a Büchner funnel until the pH of the solution reached 6–7. It was dried again in an electric furnace at 100 °C for 24 h. The action of HCl opened pores in the carbon matrix by etching the template. This procedure was found to be the most effective regarding the removal of  $\text{CaCO}_3$ . Further in the text, N-CFO-*T* is used as a unique denotation, where *T* is carbonization temperature (°C).

### Material characteristics

The N-rich CFO were examined using the low-temperature nitrogen adsorption method. The relevant isotherms of all samples were measured at –196 °C using an automatic adsorption instrument, ASAP 2010 (Micromeritics, USA). Prior to gas adsorption measurements, the carbon materials were outgassed in a vacuum at 200 °C for 2 h. The pore properties of the carbon matrixes, including the Brunauer–Emmett–Teller surface area ( $S_{\text{BET}}$ ), were determined by physical adsorption using the BET method. Based on experimental nitrogen adsorption isotherms,

differential and integral pore width distributions were calculated using the density functional theory (DFT) method. The volume of micropores ( $V_{\text{mi}}$ ) was determined based on the parameters of the Horvath–Kawazoe equation. The total pore volume ( $V_t$ ) was determined from one point for the maximum  $p/p_0$  in the adsorption isotherm. The elemental composition (carbon, nitrogen, and hydrogen) of the materials was analyzed by means of a combustion elemental analyzer (Vario MACRO CHN, Elementar Analysensysteme GmbH). The morphology of the carbons prepared from L-lysine was analyzed using scanning electron microscopy (SEM, 1430 VP, LEO Electron Microscopy Ltd.). The obtained porous carbon matrixes were also examined by high-resolution transmission electron microscopy (HRTEM, FEI Europe production, model Tecnai F20 X-Twin). X-ray photoelectron spectroscopy (XPS) measurements were performed with a VG Scientific photoelectron spectrometer ESCALAB-210 using Al K $\alpha$  radiation (1486.6 eV) from an X-ray source operating at 14.5 kV and 25 mA. Survey spectra were recorded for all the samples in the energy range from 0 to 1350 eV with 0.4 eV step. High-resolution spectra were recorded with 0.1 eV step, 100 ms dwell time, and 25 eV pass energy. A ninety-degree take-off angle was used in all measurements. Curve fitting was performed using the AVANTAGE software provided by Thermo Electron, which describes each component of the complex envelope as a Gaussian–Lorentzian sum function; a constant 0.3 ( $\pm 0.05$ ) G/L ratio was used. The background was fitted using the nonlinear Shirley model. Scofield sensitivity factors and the measured transmission function were used for quantification. The N-rich CFO was examined by Raman spectroscopy (microscope Renishaw InVia, Renishaw plc (Gloucestershire, UK), Laser: Modu-Laser Stellar-REN, Multi-Line (maximum Power 150 mW), Leica DM1300M camera Infinity 1; objective: Leica, N PLAN L50x/0.5). All of the spectra were collected at ambient temperatures.

### Electrochemical measurements

The ORR activity was electrochemically evaluated with a rotating disk electrode (RDE). Electrochemical measurements were executed using an Autolab electrochemical workstation (PGSTAT128N, Netherlands), with a standard three-electrode system, in an electrolyte solution of 0.1 M KOH at room

temperature (KOH was purchased from POCH, KOH content min. 85%). A glassy carbon electrode (GCE, 3 mm diameter), an Ag/AgCl electrode in 3 M KCl, and Pt wire were used as a working electrode, reference electrode, and counter electrode, respectively. A commercial platinum on graphitized carbon Pt/C (20 wt% platinum) catalyst was acquired from Sigma-Aldrich. 2.5 mg of the catalyst was suspended in 0.5 ml of distilled water, isopropanol, and Nafion (0.5 wt% Nafion) to form a homogeneous ink through ultrasonication for 60 min. Afterward, 5.63  $\mu\text{l}$  of the catalyst ink was dropped using a pipette onto the pre-polished glassy carbon electrode (GCE) and then dried. The catalyst loading amount was approximately  $0.4 \text{ mg cm}^{-2}$ . The ORR activity of the samples was evaluated via cyclic voltammetry (CV) at a scan rate of  $10 \text{ mV s}^{-1}$ , as well as linear sweep voltammetry (LSV) at a scan rate of  $5 \text{ mV s}^{-1}$ , in an electrolyte solution of 0.1 M KOH, using a RDE system (Metrohm, Netherland). The LSV curves were obtained at rotation speed of 1600 rpm, in an oxygen-saturated electrolyte solution. All the experiments were conducted at room temperature. The number of electrons ( $n$ ) involved in the ORR can be deduced from the Koutecky–Levich ( $K$ – $L$ ) equation:

$$J^{-1} = J_L^{-1} + J_K^{-1} = \left( B\omega^{1/2} \right)^{-1} + J_K^{-1} \quad (1)$$

$$B = 0.62nFC_0(D_0)^{2/3}\nu^{-1/6} \quad (2)$$

where  $J$ ,  $J_L$ , and  $J_K$  are the measured, diffusion limiting, and kinetic current density;  $\omega$  is the angular velocity of the disk;  $n$  is the number of transferred electrons in the reaction;  $F$  is the Faraday constant ( $96485 \text{ C mol}^{-1}$ );  $C_0$  is the concentration of dissolved oxygen in the 0.1 M KOH ( $1.2 \times 10^{-6} \text{ mol L}^{-1}$ );  $D_0$  is the diffusion coefficient of dissolved oxygen in the 0.1 M KOH ( $1.9 \times 10^{-5} \text{ cm}^2 \text{ s}^{-1}$ );  $\nu$  is the kinetic viscosity of the 0.1 M KOH ( $0.01 \text{ cm}^2 \text{ s}^{-1}$ ) [7]. According to Eqs. (1) and (2),  $n$  can be obtained from the slope of the  $K$ – $L$  plot.

All the ORR currents presented in the figures are Faradaic currents, after correction for the capacitive current. For Tafel plots, the kinetic current was determined after mass-transport correction of RDE curves by:

$$J_K = (J * J_L) / (J_L - J) \quad (3)$$

## Results and discussion

The goal of the manufacturing procedure was the synthesis of carbon foams, i.e., a specific material in which the size of pores exceeds the thickness of walls. Electron microscopy SEM and HRTEM are useful tools for identifying the occurrence of a foam-like structure. As a reference material, carbonized raw L-lysine was examined and obtained without a template. The representative images from microscopic analysis prove that carbons produced from amino acids without a template had flat and non-porous structure (Fig. 1a). Since the simple carbonization of raw amino acids led only to the production of a non-porous carbon matrix, the template procedure seems crucial to synthesizing porous carbon, as it is one of the most effective methods of provoking the development of porosity. The effects of the carbonization temperature on the development of porous carbon materials were also investigated. The SEM images of N-CFO-700, N-CFO-800, and N-CFO-900 samples are presented in Fig. 1b–d, respectively. Carbon matrixes exhibit cavities on their external surface that may be treated as entrances to the system of interconnected, different-sized pores. The images obtained by HRTEM analysis for the N-CFO-800 sample are presented in Fig. 2 with different levels of magnification. Their shapes reflect that the grains of the template are spherical, with diameters in the range of 15–40 nm. The HRTEM images were prepared for N-CFO-800 (Fig. 2a, b) and N-CFO-900 (Fig. 2c, d) samples carbonized at 800 °C and 900 °C and clearly show the amorphous character of the produced matrixes. In contrast to typical nano-structured carbon like multi-walled carbon nanotubes or multilayered graphene, no nanoscale-assembled domains like locally stacked parallel graphene sheets are visible. The thin walls of the carbon L-lysine matrix are similar in the form of carbon foam [16]. Spherical foam walls are interconnected irregularly. The carbonization process as it was carried out transformed the amino acid into a carbon foam with very thin walls. The materials were fully cleared of calcium carbonate (etching with HCl), and no template particle residue was visible. The temperature of the carbonization process does not significantly affect the structure of the obtained carbon matrixes. It can be seen that all pores have an open structure, but some are covered with transparent hemisphere carbon film.



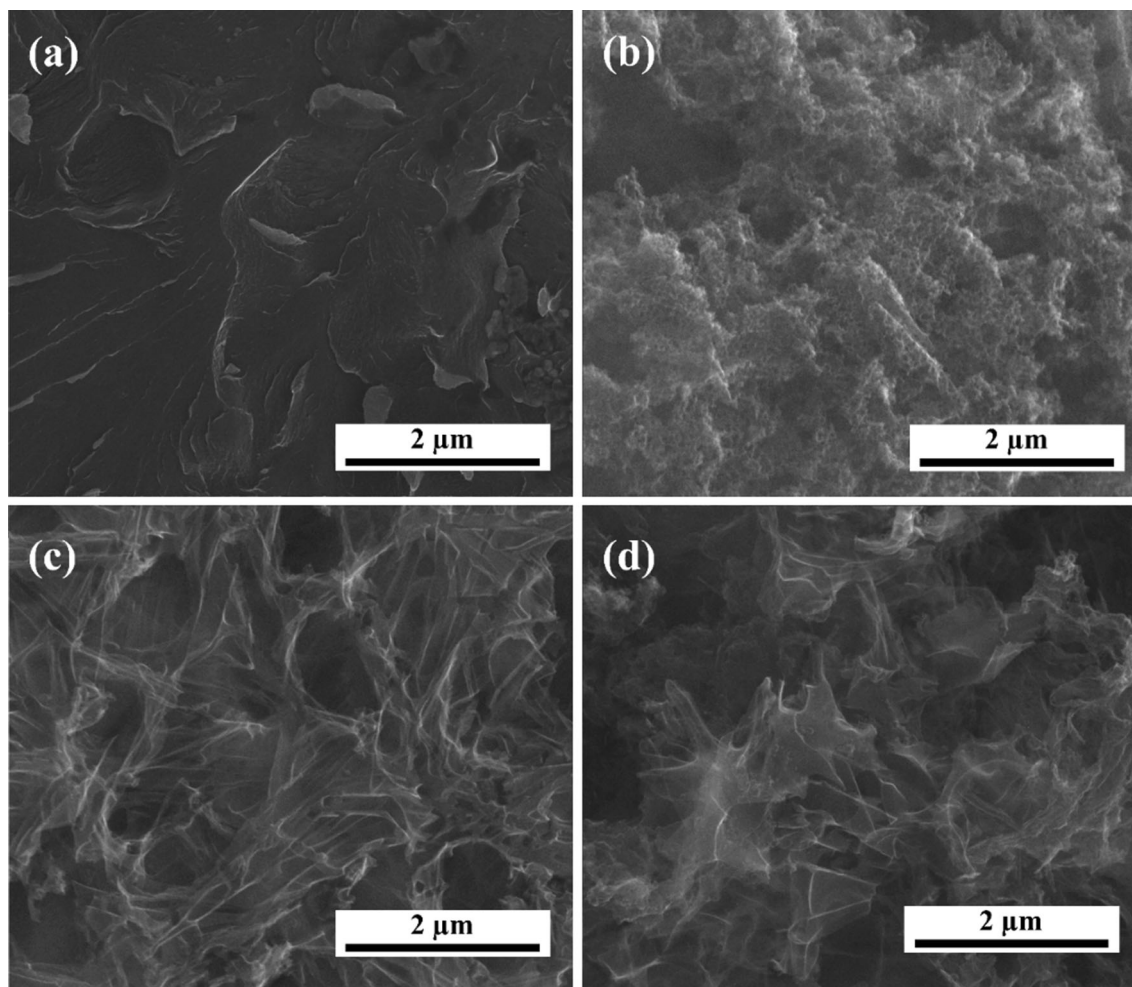


**Figure 1** SEM images of **a** unmodified L-lysine carbonized at 700 °C in N<sub>2</sub> atmosphere, **b** N-CFO-700, **c** N-CFO-800, **d** N-CFO-900.

The elemental composition and surface parameters for carbon foams prepared with a template agent are presented in Table 1. The nitrogen content in the raw precursor of L-lysine was 14.9 wt%. During N-CFO-*T* series carbonization, the heterocyclic rings formed in the first stage of pyrolysis condensed into carbon-nitrogen polycyclic structures to form a porous structure with a high nitrogen content. As is evident, the nitrogen atoms were successfully transferred from a raw amino acid to a carbon. Normally, some nitrogen contained in the precursor passes to the carbon matrix while the remaining part is released as volatile and liquid low-molecular products. Some early studies revealed that during heating to the temperature of approximately 400 °C, L-lysine has the unique property of cyclization, the formation of six-ring aromatic hydrocarbons containing nitrogen [3, 4]. Thus, the transfer of nitrogen from amino acids to carbon matrixes in N-CFO was dependent on the

N-content in the precursor and the carbonization temperature: the lower the carbonization temperature, the higher the N-transfer efficiency. As expected, the nitrogen content decreased upon increasing the carbonization temperature up to 900 °C; however, it was still very high. For the N-CFO-900 sample, nitrogen content was 4.1 wt%, about one-third of the values noted for sample N-CFO-700, where the nitrogen content was 12.4 wt%. This effect was observed in many other studies; heteroatoms like oxygen and nitrogen were progressively more intensely eliminated with the increasing carbonization temperature [34]. It has to be stated that nitrogen content is not a sole factor governing the electrochemical reduction of oxygen. There is no a direct relation between high N-content and the carbon material's ability to reduce oxygen. Thus, the observed decrease in N-content upon the carbonization temperature increase to 900 °C does not

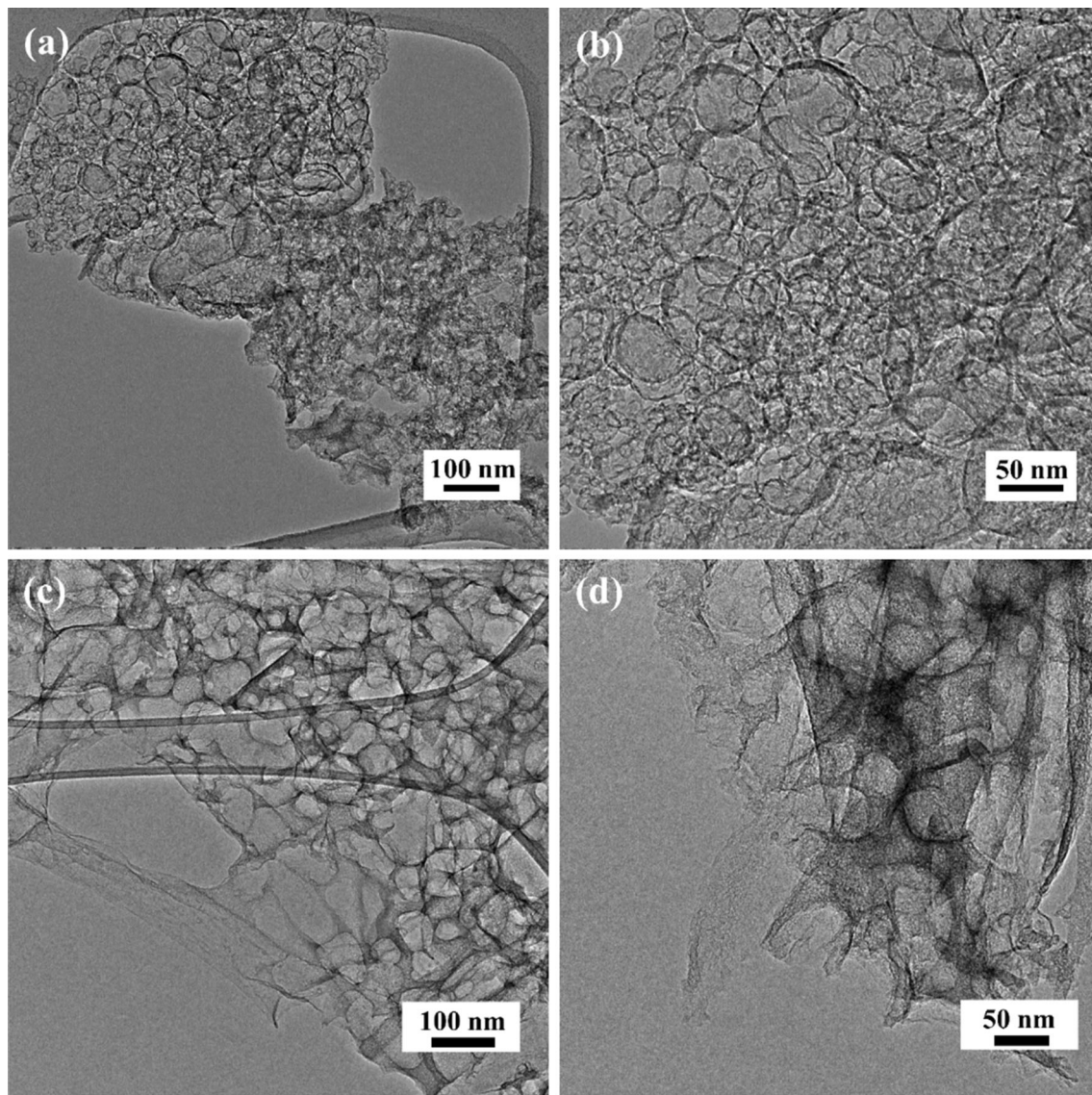


**Figure 2** HRTEM images of **a, b** N-CFO-800 and **c, d** N-CFO-900 with different magnifications.

**Table 1** Elemental composition and nitrogen physisorption properties of as-prepared porous carbons

Sample	Elemental analysis (wt%)			$S_{\text{BET}}$ ( $\text{m}^2 \text{g}^{-1}$ )	$V_{\text{mi}}$ ( $\text{cm}^3 \text{g}^{-1}$ )	$V_{\text{t}}$ ( $\text{cm}^3 \text{g}^{-1}$ )
	N	C	H			
N-CFO-700	12.4	69.6	1.9	794	0.37	0.59
N-CFO-800	9.1	76.8	1.3	1287	0.59	0.97
N-CFO-900	4.1	80.2	1.0	1125	0.49	1.09

disqualify N-CFO manufactured in the temperature range 800–900 °C as ORR active electrode material. On the other hand, the observed decrease in nitrogen content in samples at higher carbonization temperatures was not combined with an improvement of their structural parameters, like specific surface area

and total pore volume. In some papers considering conventional precursors (coconut shell, chitosan, chitin, wood, etc.), the increase in carbonization temperature and/or its extended duration resulted in the deterioration of the aforementioned structural properties. This happened above a certain threshold



temperature, due to more or less intensive graphitization of the carbon matrix [6, 11, 20, 22]. The phenomenon is observable for most heat-treated organic precursors, but in some cases the threshold temperature is particularly high and placed above 900–1000 °C. In the case of the current amino acid precursor, the threshold temperature is definitely higher than 900 °C, as opposed to, e.g., certain polymers of natural products.

The specific surface area for carbon received from raw L-lysine was below  $1 \text{ m}^2 \text{ g}^{-1}$ ; therefore, the obtained result caused the application of the template method to develop the specific surface area. The specific surface area for sample N-CFO-900 is still very high at  $1125 \text{ m}^2 \text{ g}^{-1}$ . Increasing the carbonization temperature from 700 to 800 °C significantly improved the specific surface area from 794 to  $1287 \text{ m}^2 \text{ g}^{-1}$  for N-CFO-700 and N-CFO-800, respectively (Table 1). The contribution of  $V_{\text{mi}}$  to  $V_{\text{t}}$  fell from 63% at 700 °C to 40% at an increased carbonization temperature of 900 °C, respectively. In series N-CFO-*T*, the major contribution to total pore volume could be attributed to mesopores. The low-temperature nitrogen adsorption isotherms for porous carbon matrixes obtained from L-lysine series are shown in Fig. 3a. According to the IUPAC classification [37], these isotherms were type-IV, which means a presence of mesopores along with a small amount of micropores.

The proposed template method is a promising technique to control the pore structure of the resultant carbon matrixes. Running the pore size distribution (PSD) function for L-lysine originated N-CFO (Fig. 3b) revealed maxima both in the range of micropores and mesopores. As follows, micropores (maxima placed at 0.7–0.9 nm and 1.2–1.3 nm), as well as small (maximum placed at 2–3 nm) and large (maximum placed at 20–50 nm) mesopores, were found in the N-CFO-*T* series.

The carbon–carbon bonding of carbon foams derived from amino acids was further probed by Raman spectra. Figure 3c shows the Raman spectra of all obtained N-rich CFO excited at a 532 nm laser line. There are differences in the intensity of signals in the analyzed series. The most intense bands were found in the spectral region between 500 and  $3000 \text{ cm}^{-1}$ ; the spectra show two main bands at  $1342 \text{ cm}^{-1}$  (D-band) and  $1585 \text{ cm}^{-1}$  (G-band). The D-band is associated with the structure of  $sp^2$ -distortions of partially disordered carbon, while the

G-band is common to all  $sp^2$  carbon forms [1, 9]. A peak at  $2975 \text{ cm}^{-1}$  (2D-band) is ascribed to a  $\text{CH}_2$  asymmetric stretching group. Figure 3c depicts an increase in the intensity ratio of the D and G bands ( $I_{\text{D}}/I_{\text{G}}$ ) linked with the increase in pyrolysis temperature. A  $I_{\text{D}}/I_{\text{G}}$  ratio increasing up till a pyrolysis temperature of 900 °C could be indicative of the presence of more in-plane heteroatoms (graphitic-like), which was confirmed by XPS results presented in Table 2. The intensity ratio of the D and G bands ( $I_{\text{D}}/I_{\text{G}}$ ) is an important parameter that can reveal the degree of graphitization. Therefore, the second effect which should be taken into consideration is the increasing graphitization degree occurring at elevated heat-treatment temperatures. It is commonly accepted that the decrease in  $I_{\text{D}}/I_{\text{G}}$  ratio corresponds to a higher graphitization degree of a carbonaceous material.

Most applications of porous carbon matrixes rely on the materials surface properties. For this reason, the surface elemental composition of the obtained matrixes was determined by means of X-ray photoelectron spectroscopy (XPS). The chemical state of nitrogen, carbon, and oxygen atoms in XPS spectra of the N-CFO-700 (Fig. 3d–f) and N-CFO-800 samples is shown in detail in Table 2. High-resolution XPS C1s spectra confirm the existence of five different carbon peaks, centered at 284.5, 285.6, 286.7, 287.9, and 290.3 eV, which can be attributed to the  $sp^2$  C (C-1),  $sp^3$  C (C-2), C–O (C-3), C=O (C-4), and O=C–O (C-5), respectively. An analysis of N1s spectra confirms that nitrogen atoms were assigned to three peaks. It revealed the presence of the following nitrogen forms: pyridinic nitrogen (N-6 at 398.3 eV), pyrrolic nitrogen (N-5 at 400.3 eV), and pyridine-N-oxide (N-X at 403–405 eV). The total amount of nitrogen in samples N-CFO-700, N-CFO-800 and N-CFO-900 was 9.3, 6.8 and 3.4 at.%, respectively. In all the analyzed samples, the two dominant nitrogen forms were the pyridinic and pyrrolic groups. The content of those main nitrogen groups is in the range from 89 to 95% in the total nitrogen content. It was observed that the carbonization temperature influenced the nitrogen content in terms of quality. An analysis of O1s spectra suggested that oxygen is present in several possible connections. The two main peaks on O1s spectra are signed as O-1 (at 530.1 eV) and O-2 (at 532.2 eV).

In recent years, N-rich porous carbons have shown potential for application as electrocatalysts for the ORR. However, there are still many challenges to

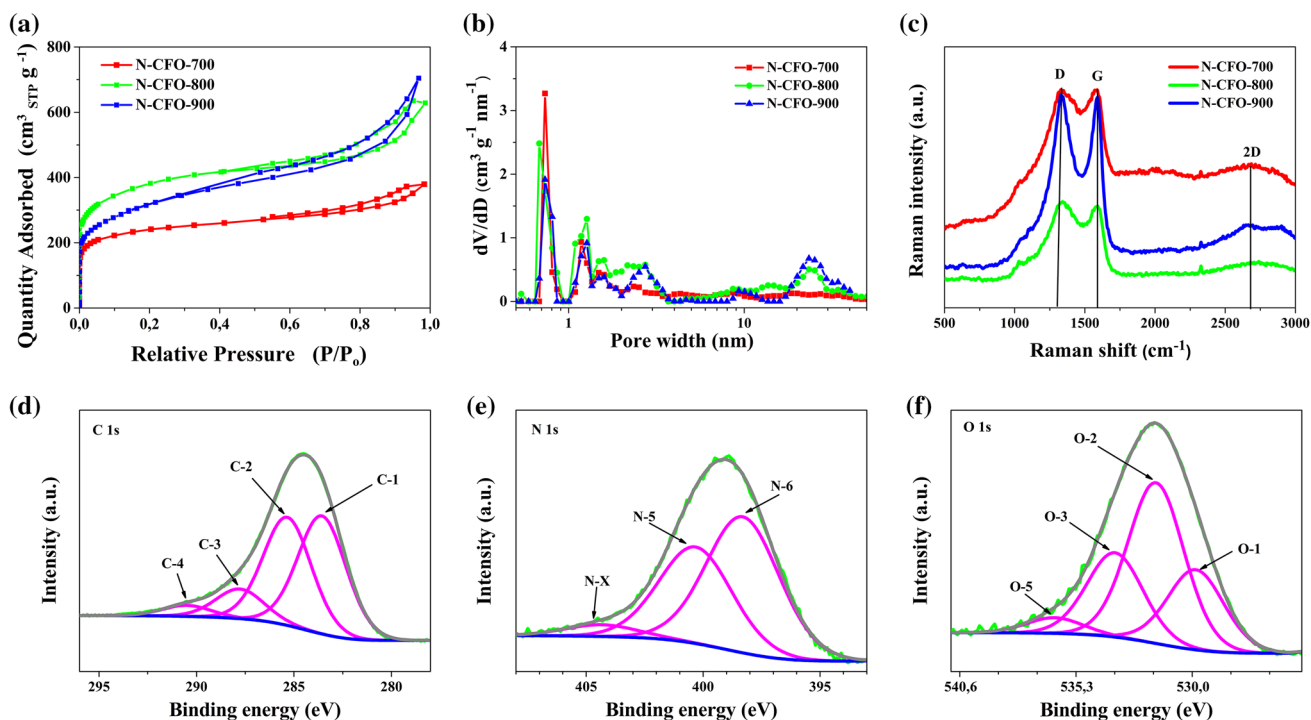


**Figure 3** **a** Nitrogen adsorption–desorption isotherms. **b** Pore size distributions calculated from  $N_2$  desorption isotherm. **c** Raman spectra of N-CFO-*T*. **d–f** The deconvoluted high-resolution C 1s, N 1s, and O 1s XPS spectra of N-CFO-700.

**Table 2** Elemental quantification analysis of N-CFO-*T* catalysts determined by XPS analysis

Peak	Content (at.%)		
	N-CFO-700	N-CFO-800	N-CFO-900
C1s (C-1)	34.9	42.2	50.2
C1s (C-2)	32.2	29.2	22.5
C1s (C-3)	8.8	8.5	10.0
C1s (C-4)	3.3	–	5.2
C1s (C-5)	–	3.6	4.2
C1s (C-6)	–	–	2.0
N1s (N-6)	5.2	3.4	1.30
N1s (N-5)	3.7	2.8	1.60
N1s (N-X)	0.4	0.6	0.50
O1s (O-1)	2.8	2.8	1.4
O1s (O-2)	5.3	4.7	1.2
O1s (O-3)	2.8	–	–
O1s (O-4)	–	1.8	–
O1s (O-5)	0.5	0.4	–

studying their structure–property relation, owing to limited rational preparation methods and poor control over the N-content in these methods. In this work, the electrocatalytic activity of N-rich carbon foams N-CFO-*T* series and Pt/C commercial

electrocatalyst was tested using cyclic voltammetry curve and linear sweep voltammetry in an electrolyte solution of 0.1 M KOH saturated with oxygen. The ORR performance was evaluated using a standard three-electrode cell. The first to be examined was the ORR activity of the N-CFO series, prepared from L-lysine and  $CaCO_3$ , as a function of carbonization temperature in the range of 700–900 °C. CV experiments were performed to investigate the electrocatalytic activity of the as-prepared samples for ORR in  $N_2$ -saturated and  $O_2$ -saturated electrolyte solution of 0.1 M KOH at a scan rate of  $10 \text{ mV s}^{-1}$ . The corresponding voltammograms are shown in Fig. 4. In the  $O_2$ -saturated condition, a characteristic cathodic peak can be observed for all samples, confirming that all nitrogen-rich samples have electrocatalytic activities for ORR. A cathodic peak appeared in the CV as the electrolyte solution was saturated with  $O_2$ . Among them, N-CFO-900 has the largest peak current density, implying arguably higher activity compared with those of N-CFO-800 and N-CFO-700 for ORR.

The linear sweep voltammograms were conducted to further understand the ORR performance of the as-prepared samples. Further analysis of the ORR kinetics for carbon foam was performed with fully saturated LSV curves (Fig. 5a). They were carried out



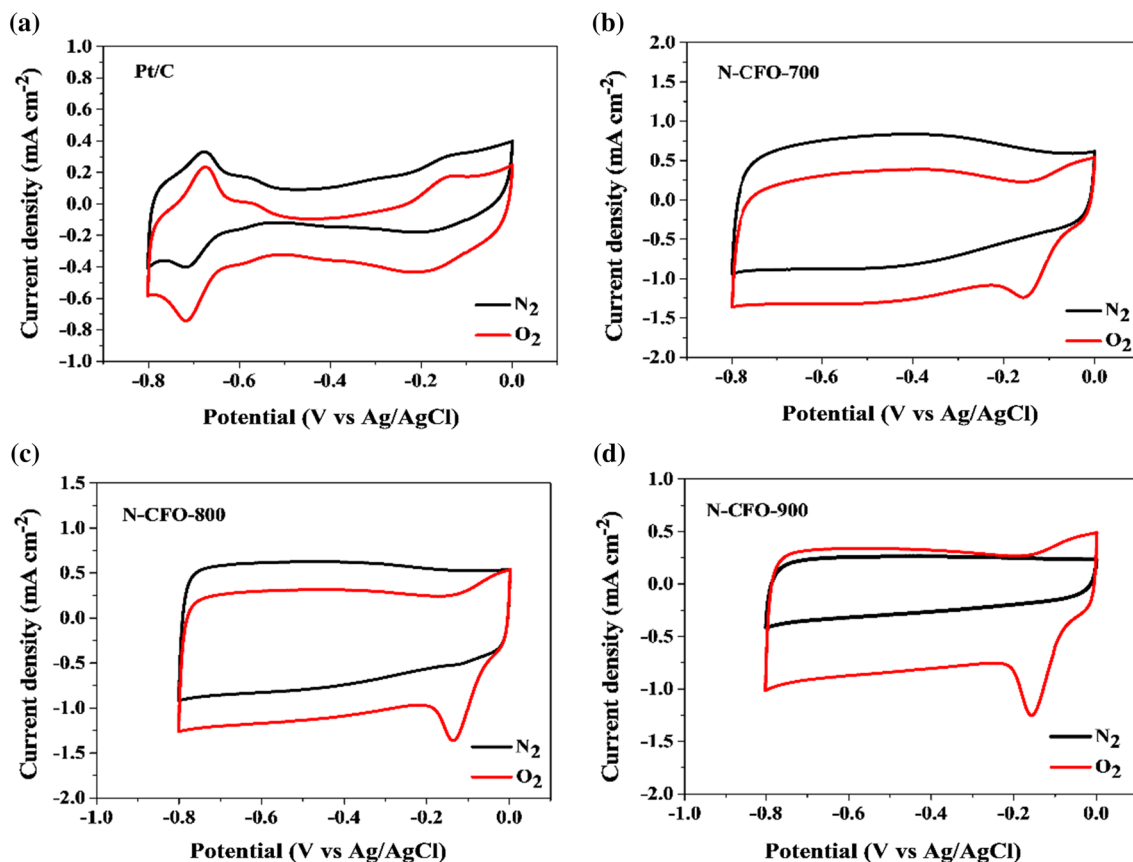


**Figure 4** Cyclic voltammograms under  $N_2$ -saturated and  $O_2$ -saturated 0.1 M KOH at the scan rate  $10 \text{ mV s}^{-1}$  of a Pt/C, b N-CFO-700, c N-CFO-800, d N-CFO-900.

in an  $O_2$ -saturated electrolyte solution of 0.1 M KOH at a rotation of 1600 rpm and a scan rate of  $5 \text{ mV s}^{-1}$ . The LSV is given in Fig. 5a and clearly shows that ORR activity was lower for the N-CFO-700 sample than for the N-CFO-800 and N-CFO-900 sample. This can probably be attributed to its low conductivity associated with a lower carbon content (Table 1) and decreasing specific surface area compared to other samples carbonized at 700 °C and 800 °C. The analysis of LSV curves allows the selection of two samples N-CFO-800 and N-CFO-900 for further analysis ( $K-L$  plots and number of transferred electrons in ORR).

The onset potential for the ORR is an important criterion in evaluating the activity of an electrocatalyst. The N-CFO-700 sample shows the onset potential of 0.91 V (Fig. 5b). Nevertheless, the N-CFO-800 and N-CFO-900 show the best activity from series N-CFO- $T$  with the same and most positive onset potential of 0.93 V, which is close to onset potential of commercial Pt/C (0.98 V). Figure 5b shows for

N-CFO-900 a more positive shift in the onset potential closer to that of commercial Pt/C. Considering the same morphology of the N-CFO series, the enhanced ORR activity can be attributed to the porosity and high content of nitrogen. However, the onset potential of N-CFO-900 is still approximately 28 mV lower than the onset potential of Pt/C. The positive effect for ORR of N-CFO-800 and N-CFO-900 is attributed to active sites from N-groups on the carbon foam surface. These results indicated that the increased specific surface area of N-CFO can enhance ORR activity. As most of the previously noted studies report, the onset ORR potential remained nearly constant despite rotation rate changes, but the measured current density showed a typical increase with an increased rotation rate due to faster oxygen flux to the electrode surface. An onset potential that is a little bit lower than that of a Pt/C catalyst was registered (Fig. 5b). Indeed, the enhanced electrocatalytic performance of N-CFO-900 was well-aligned with the physiochemical analysis. The N-rich carbon foams

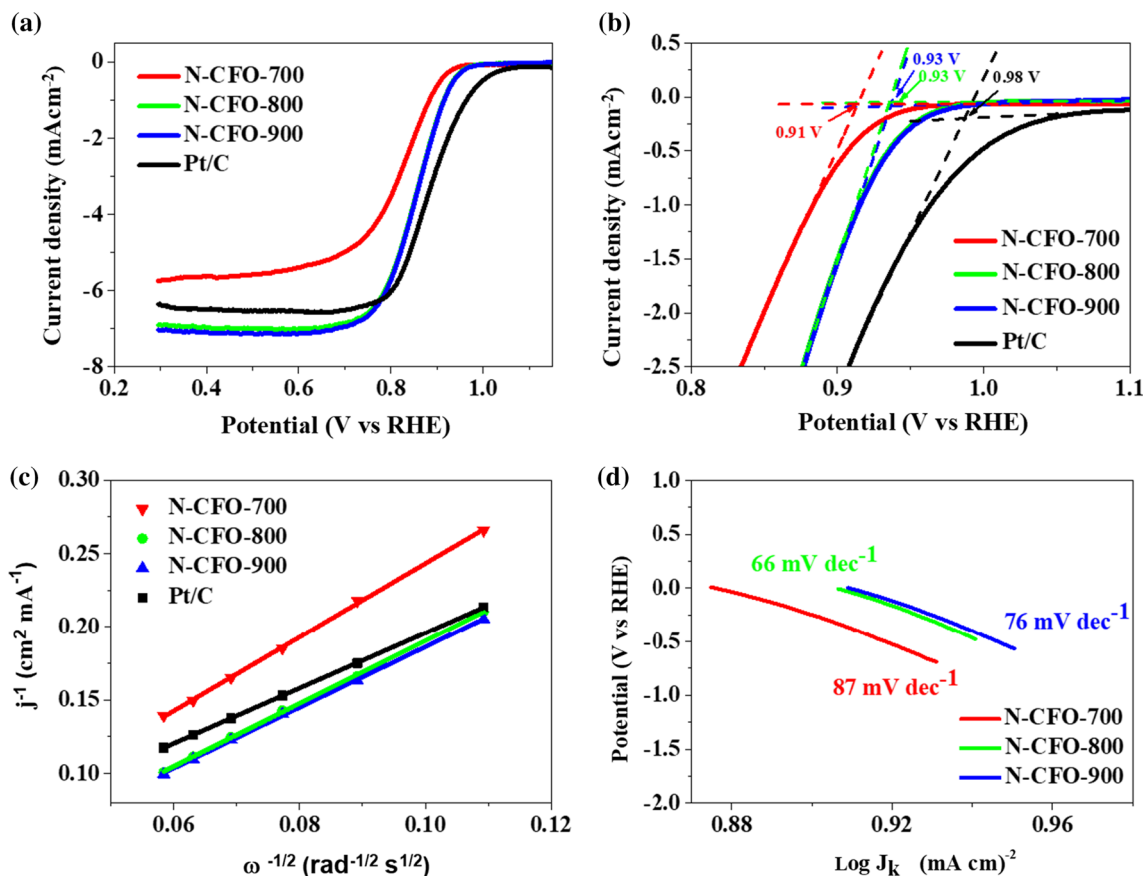


**Figure 5** **a** Linear sweep voltammogram curves of N-CFO-*T* and Pt/C at a rotation speed of 1600 rpm. **b** Onset potential determination in expanded LSV curves. **c** The Koutecky–Levich

plots corresponding to the hydrodynamic voltammograms at 0.5 V. **d** Tafel plots derived from LSV curves.

showed a various activity, which could be attributed to the effect of carbonization temperature, N-doping and porosity. In this regard, carbonization of N-rich carbon foam at 900 °C seems to define an ideal carbonization temperature to generate a carbocatalyst with a probable balance of porosity, surface area, and sufficient active catalytic sites promoted by pyridinic and pyrrolic nitrogen. The high specific surface area and micro-, mesoporous structure both facilitate gas and electrolyte diffusion of ORR. The half-wave potential for N-CFO-700, N-CFO-800, N-CFO-900 and Pt/C is 0.84 V, 0.86 V, 0.86 V and 0.89 V, respectively.

Figure 5c shows good linear fitting of *K*–*L* plots at potential of 0.5 V for all analyzed samples. The transferred electron number (*n*) was calculated based on RDE measurements. These two N-CFO samples demonstrated the same trend: *n* increased with the increase in overpotential. *n* values were close to 4, implying a four-electron pathways for ORR. The

number of electron transfers for CFO-800 and N-CFO-900 ranged between 3.5 and 4, being similar to the Pt/C reference catalyst. The *n* value for N-CFO-800 and N-CFO-900 is suggesting that four electron reduction mechanism occurs, marking high activity for ORR. When comparing N-CFO-800 and N-CFO-900, a very similar number of electron transfer is observable, although the N-content is different at 9.1 and 4.1 wt%, respectively. As expected, the physical morphology of these two samples is comparable, 1287 m<sup>2</sup> g<sup>−1</sup> for N-CFO-800 and 1125 m<sup>2</sup> g<sup>−1</sup> for N-CFO-900. It is understood that the N-CFO-800 and N-CFO-900 samples have similar activities for ORR due to similar porosity. The high surface area and a high contribution of mesopores to the total pore volume provide a full exposure of active sites of these two samples facilitate electron transfer which is critical for achieving high catalytic ORR activity. Moreover, carbonization temperature of 800–900 °C

provided high electric conductivity to such N-CFOs resulting from more intensive graphitization process.

The Koutecky–Levich ( $K-L$ ) equation was used to analyze the RDE data. As shown in Fig. 5c, the corresponding  $K-L$  plots showed good linearity and were nearly parallel at various potentials, which revealed first-ordered reaction kinetics with respect to the concentration of dissolved  $O_2$ . The Tafel slopes (Fig. 5d) were estimated to be about  $87 \text{ mV dec}^{-1}$  for the N-CFO-700,  $66 \text{ mV dec}^{-1}$  for the N-CFO-800 and  $76 \text{ mV dec}^{-1}$  for the N-CFO-900 (Fig. 5d). It was noted the Tafel slope of the N-CFO-700 was the lowest among all of the as-prepared N-CFO- $T$  catalysts. However, the N-CFO-800 and N-CFO-900 samples show much better activities for ORR than N-CFO-700 because of their higher specific surface area and still high amounts of nitrogen, which are important influences over ORR performance. Nonetheless, N-CFO-900 exhibits the best activity among the as-prepared samples with a lesser amount of nitrogen, less than of N-CFO-700, implying that there is a factor besides the amount of the nitrogen that is responsible for the high activity for ORR, porosity and carbonization temperature plays a crucial role. The results suggest that the N-CFO- $T$  series has approached catalytic activity for ORR to the commercial Pt/C catalyst. Therefore, metal-free catalyst prepared from L-lysine as a carbon and nitrogen source could be applied as a good alternative to commercial Pt/C electrocatalyst for ORR, a key reaction in the practical application of metal-air batteries.

## Conclusions

Presented in this study was the effective synthesis of nitrogen-rich porous carbon foams (N-CFO) from L-lysine as a carbon precursor. The pore structure of N-CFO was created by adding  $CaCO_3$  in the form of large insoluble nanoparticles of sizes between 15 and 40 nm, and etching after carbonization. All experiments (based on the hard template method) intended to reduce wall thickness and achieve the highest possible nitrogen content in corresponding N-CFO. The nitrogen content was very high, placing itself in the range of 4.1–12.4 wt%. The BET surface area was in the range of  $794\text{--}1287 \text{ m}^2 \text{ g}^{-1}$ . The structure and electrocatalytic activity of N-rich carbon foam were also investigated. The decrease in  $I_D/I_C$  ratio

corresponds to a higher graphitization degree of a carbonaceous material. It was documented that N-content is not a sole factor determining the effectiveness of ORR performed by N-CFO electrodes. The decrease in N-content upon the increase in carbonization temperature did not reduce the activity of N-CFO-based electrodes in ORR. The benefits of the presented exceptional features include a simple and convenient preparation procedure, as well as an easily accessible raw material (amino acid). The good catalytic activity of the N-CFO- $T$  series can most likely be attributed to a high specific surface area, a high contribution of mesopores to the total pore volume and electrochemical nitrogen catalytic sites. Moreover, the particular pore architecture and high specific surface area are beneficial to expose more potential active centers to the electrolyte and facilitate the rapid electron transport and oxygen diffusion; therefore, the available active catalytic sites enhance the catalytic activity.

## Compliance with ethical standards

**Conflict of interest** The authors declare no conflict of interests.

**Open Access** This article is distributed under the terms of the Creative Commons Attribution 4.0 International License (<http://creativecommons.org/licenses/by/4.0/>), which permits unrestricted use, distribution, and reproduction in any medium, provided you give appropriate credit to the original author(s) and the source, provide a link to the Creative Commons license, and indicate if changes were made.

## References

- [1] Beltrame KK, Cazetta AL, de Souza PSC, Spessato L, Silva TL, Almeida VC (2018) Adsorption of caffeine on mesoporous activated carbon fibers prepared from pineapple plant leaves. *Ecotoxicol Environ Saf* 147:64–71
- [2] Borghei M, Laocharoen N, Kibena-Pöldsepp E, Johansson L-S, Campbell J, Kauppinen E, Tammeveski K, Rojas OJ (2017) Porous N, P-doped carbon from coconut shells with high electrocatalytic activity for oxygen reduction: alternative to Pt-C for alkaline fuel cells. *Appl Catal B* 204:394–402
- [3] Breitbart DJ, Nawar WW (1979) Thermal decomposition of lysine. *J Agric Food Chem* 27:511–514



- [4] Bryan AM, Olafsson PG (1969) Analysis of thermal decomposition patterns of aromatic and heteroaromatic amino acids. *Anal Lett* 2:505–513
- [5] Chen T, Dai L (2013) Carbon nanomaterials for high-performance supercapacitors. *Mater Today* 16:272–280
- [6] Cyganiuk A, Gorska O, Olejniczak A, Lukaszewicz JP (2012) Pyrolytic production of microporous charcoals from different wood resources. *J Anal Appl Pyrol* 98:15–21
- [7] Davis RE, Horvath GL, Tobias CW (1967) The solubility and diffusion coefficient of oxygen in potassium hydroxide solutions. *Electrochim Acta* 12:287–297
- [8] Fan H, Shen W (2016) Gelatin-based microporous carbon nanosheets as high performance supercapacitor electrodes. *ACS Sustain Chem Eng* 4:1328–1337
- [9] Gao Y, Yue Q, Xu S, Gao B, Li Q, Yu H (2015) Preparation and evaluation of adsorptive properties of micro-mesoporous activated carbon via sodium aluminate activation. *Chem Eng J* 274:76–83
- [10] Ghosh A, Ghosh S, Seshadhri GM, Ramaprabhu S (2019) Green synthesis of nitrogen-doped self-assembled porous carbon-metal oxide composite towards energy and environmental applications. *Sci Rep* 9:1–13
- [11] Ilnicka A, Lukaszewicz JP (2015) Synthesis of N-rich microporous carbon materials from chitosan by alkali activation using  $\text{Na}_2\text{CO}_3$ . *Mater Sci Eng B* 201:66–71
- [12] Ilnicka A, Gauden PA, Terzyk AP, Lukaszewicz JP (2016) Nano-structured carbon matrixes obtained from chitin and chitosan by a novel method. *J Nanosci Nanotechnol* 16:2623–2631
- [13] Ilnicka A, Kamedulski P, Lukaszewicz JP (2017) Pyrolysis of *Chlorella vulgaris* as a green chemistry method for manufacturing of nitrogen doped porous carbon materials of high application potential. *Mater Express* 7:1–10
- [14] Inagaki M, Morishita T, Kuno A, Kito T, Hirano M, Suwa T, Kusakawa K (2004) Carbon foams prepared from polyimide using urethane foam template. *Carbon* 42:497–502
- [15] Inagaki M, Kang F, Toyoda M, Konno H (2014) Chapter 9: carbon foams. In: Inagaki M, Kang F, Toyoda M, Konno H (eds) *Advanced materials science and engineering of carbon*. Butterworth-Heinemann, Boston, pp 189–214
- [16] Inagaki M, Qiu J, Guo Q (2015) Carbon foam: preparation and application. *Carbon* 87:128–152
- [17] Jiang H, Liu Y, Hao J, Wang Y, Li W, Li J (2017) Self-assembly synthesis of cobalt-and nitrogen-coembedded trumpet flower-like porous carbons for catalytic oxygen reduction in alkaline and acidic media. *ACS Sustain Chem Eng* 5:5341–5350
- [18] Jiang H, Liu Y, Li W, Li J (2018) Co nanoparticles confined in 3D nitrogen-doped porous carbon foams as bifunctional electrocatalysts for long-life rechargeable Zn–air batteries. *Small* 14:1–10
- [19] Jiang H, Gu J, Zheng X, Liu M, Qiu X, Wang L, Li W, Chen Z, Ji X, Li J (2019) Defect-rich and ultrathin N doped carbon nanosheets as advanced trifunctional metal-free electrocatalysts for the ORR, OER and HER. *Energy Environ Sci* 12:322–333
- [20] Katesa J, Junpiromand S, Tangsathitkulchai C (2013) Effect of carbonization temperature on properties of char and activated carbon from coconut shell. *Suranaree J Sci Technol* 20:269–278
- [21] Kucinska A, Cyganiuk A, Lukaszewicz JP (2012) A microporous and high surface area active carbon obtained by the heat-treatment of chitosan. *Carbon* 50:3098–3101
- [22] Kucińska A, Gołębiewski R, Łukaszewicz JP (2013) Węgle aktywne wzbogacone w azot otrzymywane z naturalnego polimeru – chityny. *Diagnozowanie Stanu Środowiska Metody Badawcze - Prognozy*, Bydgoszcz, pp 185–201
- [23] Lezanska M, Olejniczak A, Rokicinska A, Kustrowski P, Lukaszewicz J (2017) Type A and B gelatin as precursors of silica-templated porous carbon with a specified number of nitrogen-and oxygen-containing functionalities. *Mater Express* 7:123–133
- [24] Li N, Chen Z, Ren W, Li F, Cheng H-M (2012) Flexible graphene-based lithium ion batteries with ultrafast charge and discharge rates. *Proc Natl Acad Sci USA* 109:17360–17365
- [25] Li Y, Shen B, Pei X, Zhang Y, Yi D, Zhai W, Zhang L, Wei X, Zheng W (2016) Ultrathin carbon foams for effective electromagnetic interference shielding. *Carbon* 100:375–385
- [26] Lin Z, Waller G, Liu Y, Liu M, Wong CP (2012) Facile synthesis of nitrogen-doped graphene via pyrolysis of graphene oxide and urea, and its electrocatalytic activity toward the oxygen-reduction reaction. *Adv Energy Mater* 2:884–888
- [27] Liu H, Li T, Wang X, Zhang W, Zhao T (2014) Preparation and characterization of carbon foams with high mechanical strength using modified coal tar pitches. *J Anal Appl Pyrol* 110:442–447
- [28] Liu J, Zhu Y, Li X, Du F, Wang R, Jiang L (2019) Three-dimensional Fe, N-doped carbon nanosheets on interconnected carbon skeletons as a highly efficient and stable electrocatalyst for oxygen reduction reaction. *J Alloys Compd* 788:1274–1281
- [29] Liu YZ, Li YF, Yuan SX, Chen S, Wang CW, Li XM, Su FY, Chen CM (2018) Synthesis of 3D N, S dual-doped porous carbons with ultrahigh surface areas for highly efficient oxygen reduction reactions. *ChemElectroChem* 5:3506–3513

- [30] Mahmood N, Zhang C, Yin H, Hou Y (2014) Graphene-based nanocomposites for energy storage and conversion in lithium batteries, supercapacitors and fuel cells. *J Mater Chem A* 2:15–32
- [31] Nagel B, Pusz S, Trzebiecka B (2014) Review: tailoring the properties of macroporous carbon foams. *J Mater Sci* 49:1–17. <https://doi.org/10.1007/s10853-013-7678-x>
- [32] Olejniczak A, Lezanska M, Wloch J, Kucinska A, Lukaszewicz JP (2013) Novel nitrogen-containing mesoporous carbons prepared from chitosan. *J Mater Chem A* 1:8961–8967
- [33] Priyanka M, Saravanakumar MP (2017) A short review on preparation and application of carbon foam. *IOP Conf Ser Mater Sci Eng* 263:1–5
- [34] Shen W, Li Z, Liu Y (2008) Surface chemical functional groups modification of porous carbon. *Recent Pat Chem Eng* 1:27–40
- [35] Soloveichik GL (2014) Liquid fuel cells. *Beilstein J Nanotechnol* 5:1399–1418
- [36] Steckle WP Jr (1996) Carbon foams prepared from hypercrosslinked polymer foams. American Chemical Society, Washington, DC, pp 26–36
- [37] Thommes M, Kaneko K, Neimark AV, Olivier JP, Rodriguez-Reinoso F, Rouquerol J, Sing KS (2015) Physisorption of gases, with special reference to the evaluation of surface area and pore size distribution (IUPAC technical report). *Pure Appl Chem* 87:1051–1069
- [38] Wang J, Ma R, Zhou Z, Liu G, Liu Q (2015) Magnesiothermic synthesis of sulfur-doped graphene as an efficient metal-free electrocatalyst for oxygen reduction. *Sci Rep* 5:1–9
- [39] Wang J, Shen L, Nie P, Yun X, Xu Y, Dou H, Zhang X (2015) N-doped carbon foam based three-dimensional electrode architectures and asymmetric supercapacitors. *J Mater Chem A* 3:2853–2860
- [40] Wang R, Chen Z, Hu N, Xu C, Shen Z, Liu J (2018) Nanocarbon-based electrocatalysts for rechargeable aqueous Li/Zn-air batteries. *ChemElectroChem* 5:1745–1763
- [41] Wöckel L, Seifert A, Mende C, Roth-Panke I, Kroll L, Spange S (2017) Resin and carbon foam production by cationic step-growth polymerization of organic carbonates. *Polym Chem* 8:404–413
- [42] Wood KN, O'Hayre R, Pylypenko S (2014) Recent progress on nitrogen/carbon structures designed for use in energy and sustainability applications. *Energy Environ Sci* 7:1212–1249
- [43] Xian F, Gao L, Zhang Z, Zhang H, Dong S, Cui G (2019) N, P dual-doped multi-wrinkled nanosheets prepared from the egg crude lecithin as the efficient metal-free electrocatalyst for oxygen reduction reaction. *Appl Surf Sci* 476:76–83
- [44] Xiao K, Zeng Y, Long J, Chen H, Ding L-X, Wang S, Wang H (2017) Highly compressible nitrogen-doped carbon foam electrode with excellent rate capability via a smart etching and catalytic process. *ACS Appl Mater Interfaces* 9:15477–15483
- [45] Xue Y, Liu J, Chen H, Wang R, Li D, Qu J, Dai L (2012) Nitrogen-doped graphene foams as metal-free counter electrodes in high-performance dye-sensitized solar cells. *Angew Chem Int Ed* 51:12124–12127
- [46] Xue Y, Yu D, Dai L, Wang R, Li D, Roy A, Lu F, Chen H, Liu Y, Qu J (2013) Three-dimensional B, N-doped graphene foam as a metal-free catalyst for oxygen reduction reaction. *Phys Chem Chem Phys* 15:12220–12226
- [47] Yuan Y, Ding Y, Wang C, Xu F, Lin Z, Qin Y, Li Y, Yang M, He X, Peng Q (2016) Multifunctional stiff carbon foam derived from bread. *ACS Appl Mater Interfaces* 8:16852–16861
- [48] Zhang H, Lv K, Fang B, Forster MC, Dervişoğlu R, Andreas LB, Zhang K, Chen S (2018) Crucial role for oxygen functional groups in the oxygen reduction reaction electrocatalytic activity of nitrogen-doped carbons. *Electrochim Acta* 292:942–950
- [49] Zhang J, Qu L, Shi G, Liu J, Chen J, Dai L (2016) N, P-codoped carbon networks as efficient metal-free bifunctional catalysts for oxygen reduction and hydrogen evolution reactions. *Angew Chem Int Ed* 55:2230–2234
- [50] Zhao Y, Liu J, Hu Y, Cheng H, Hu C, Jiang C, Jiang L, Cao A, Qu L (2013) Highly compression-tolerant supercapacitor based on polypyrrole-mediated graphene foam electrodes. *Adv Mater* 25:591–595
- [51] Zheng Y, Jiao Y, Li LH, Xing T, Chen Y, Jaroniec M, Qiao SZ (2014) Toward design of synergistically active carbon-based catalysts for electrocatalytic hydrogen evolution. *ACS Nano* 8:5290–5296
- [52] Zhou Z, Zhang H, Zhou Y, Qiao H, Gurung A, Naderi R, Elbohy H, Smirnova AL, Lu H, Chen S (2017) Binder free hierarchical mesoporous carbon foam for high performance lithium ion battery. *Sci Rep* 7:1–9

**Publisher's Note** Springer Nature remains neutral with regard to jurisdictional claims in published maps and institutional affiliations.